



Computational Analysis on the Performance of Centrifugal Compressor with Tapered Wall and Rotating Tapered Wall Vaneless Diffuser

P. Niveditha[†] and B. V. S. S. Prasad

Indian Institute of Technology, Madras, Tamilnadu 600032, India

[†]*Corresponding Author Email: nivvu.babbi@gmail.com*

(Received July 13, 2020; accepted September 21, 2020)

ABSTRACT

Computational analysis is performed on a centrifugal compressor fitted with tapered vaneless diffuser in order to increase the rate of diffusion. The main parameter involved in the present study is the wall taper angle of the diffuser, which is varied from 1° to 6° in the interval of 1°. Simulations are performed for the stationary as well as rotating diffuser at a speed of 79,000rpm, by using ANSYS CFX 17.2. By considering the geometry with stationary parallel wall diffuser as the base case, the performance enhancement in the characteristics such as static pressure recovery coefficient, stagnation pressure loss coefficient, isentropic efficiency, energy coefficient and torque coefficient are reported. The flow features in the compressor having various diffuser geometries are studied with the help of static pressure, radial velocity, static entropy, and contours of velocity streamlines at the design point. Of all the cases of stationary tapered diffusers, the diffuser with 3° taper angle showed optimum performance: the increase in isentropic efficiency (η) is by 1.5%, the increase in static pressure recovery coefficient (C_p) is by about 9% and the decrease in stagnation pressure loss coefficient (C_{p0}) by 10.7%. On the other hand, it was found that in the case of rotating diffuser optimum performance: an increase of about 40% in C_p and decrease of about 32% in C_{p0} occurred for a taper angle of 6°. However, its efficiency decreased by 2.9% with rotating diffuser in comparison with the base case, due to increased energy losses.

Keywords: Compressor performance; Computational fluid dynamics; Rotating diffuser; Tapered diffuser; Vaneless diffuser.

NOMENCLATURE

C_{1u}	tangential velocity component at impeller inlet	S	entropy
C_{2u}	tangential velocity component at impeller outlet	S_E	energy source
C_p	static pressure recovery coefficient	S_M	momentum source
C_{p0}	stagnation pressure loss coefficient	SVD	stationary vaneless diffuser
d_m	mean diameter of diffuser	T	static temperature
fP_{02}	total pressure at impeller outlet	T_{01}	total temperature at compressor inlet
h	static enthalpy	T_2	torque at impeller outlet
h_{tot}	total enthalpy	T_3	torque at diffuser outlet
m	mass flow rate	TRVDX	X° Tapered Rotating Vaneless Diffuser
P_{01}	total pressure at compressor inlet	TSVDY	Y° Tapered Stationary Vaneless Diffuser
P_{03}	total pressure at diffuser outlet	U	velocity magnitude
P_2	static pressure at impeller outlet	U_1	peripheral velocity at impeller inlet
P_3	static pressure at diffuser outlet	U_2	peripheral velocity at impeller outlet
P_{avg}	average static pressure	U_m	mean velocity of diffuser
r	diffuser inlet radius	Z_{0_hub}	standard Z of hub, parallel wall diffuser
r_0	total pressure ratio	Z_{0_Shroud}	changed Z of shroud to model the tapered diffuser
r_{2x}	varying radius of the tapered diffuser	Z_{hub}	changed Z of hub to model the tapered diffuser
RVD	Rotating Vaneless Diffuser		

Z_{Shroud}	changed Z of hub to model the tapered diffuser	λ	thermal conductivity
μ	dynamic viscosity	ρ	density
η	isentropic efficiency of compressor	τ	shear stress
θ	taper angle of diffuser	Ψ	energy coefficient

1. INTRODUCTION

Several energy and aerospace appliances make use of centrifugal turbomachines such as pumps and compressors. Significant research efforts [Hoseinizadeh et al. \(2020a\)](#); [Barbaryan et al. \(2019\)](#); [Kohzadi et al. \(2018\)](#) are found for improving the performance of such machines or alleviating the problems occurring in them. For example, solutions to cavitation issues arising in centrifugal pumps are suggested by [Hoseinizadeh et al. \(2018b\)](#); stall and surge problems in centrifugal compressor are addressed by [Powers et al. \(2020\)](#); [Chenxing et al. \(2020\)](#).

In a centrifugal compressor, a complex three-dimensional unsteady flow occurs in the rotating impeller followed by the stationary diffuser. Centrifugal compressor may be fitted with a vaneless diffuser, vaned diffuser or both. In the case of a vaned diffuser the operating range of the centrifugal compressor is lower than the vaneless diffuser. Although the operating range of the vaneless diffuser is higher than the vaned diffuser, the resulting pressure rise is lower. In the present study an attempt has been made to increase pressure rise in the vaneless diffuser by surface modifications such as tapering and by integrating the diffuser with the impeller, refer Fig. 1.

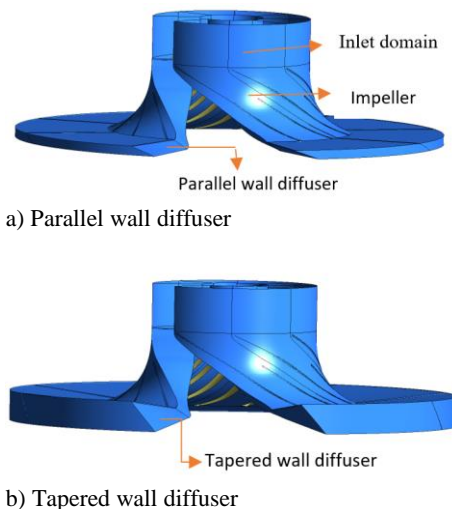


Fig. 1. Centrifugal compressor fitted with parallel wall diffuser and tapered wall diffuser.

The increase in pressure of a centrifugal compressor is attributable to the impeller's centrifugal operation and the downstream diffuser or volute's diverging passages.

[Dean et al. \(1960\)](#) had experimented by using

compressor fitted with vaneless diffuser. Authors conclude that the flow that enters the diffuser is distorted flow profile, hence the compressor performance depends on the outlet flow angle of the impeller, wall friction and degree of distortion plays a vital role in compressor performance. [Krain \(1988\)](#) had studied flow in an impeller with backswept blades. He concluded that the swirling flow in the impeller induces secondary flow and distorted flow inside the compressor fluid domain.

[Sun et al. \(2016\)](#) studied the compressor fitted with pipe diffuser. They concluded that vaneless space before vaned diffuser smoothens the distorted flow profile entering the vaned pipe diffuser.

The factors which affect the performance of the diffuser are impeller diffuser interaction, rotating stall and diffuser outflow. Since the flow from impeller to diffuser is unstable, three-dimensional and non-uniform, the design of the diffuser should be such that compressor performance will not be affected by these factors. In vaneless diffuser, rotating stall is a big problem as there are no vanes to guide the non-uniform entry diffuser from the impeller. Diffuser outflow should also be monitored without wakes, so that no losses occur in downstream flow (Volute). Earlier works done with compressor equipped vaneless diffuser are discussed below. Researchers have tried to solve above mentioned problems by increasing or decreasing the width of the diffusers and rotating diffusers. These studies are discussed below.

[Senoo et al. \(1977\)](#) had studied different inlet conditions and widths of centrifugal vaneless diffuser. They concluded the diffuser width effect is more on the diffuser flow angle. So, they also concluded that the radial velocity component has more effect on distorted flow compared to the tangential velocity component

[Lindner \(1983\)](#) had investigated effects of varying diffuser diameter ratio, axial stage pitch and blade cutback. Depending on the shaft size of the impeller, efficiency improved for higher shaft sizes by reducing axial stage pitch while by reducing axial pitch increases the number of enclosures in case of lower and medium shaft size applications, which decreases compressor efficiency. He concluded that 4.5 percent cutback offered better performance and a larger cutback of 8.75 percent showed lower compressor output. [Ferrara et al. \(2004\)](#) had performed experiments in a high-pressure ratio compressor to test rotating stall, effect of varying width and pinch shape. Various geometries of vaneless diffusers are examined with volute. The authors concluded that the diffuser working range is influenced by varying diffuser width. And they also concluded that shortening diffuser does not always

boost compressor efficiency, but rather creates problems with compressor stability.

Seven different types of diffusers were studied [Jaatinen et al. \(2011\)](#), decreasing the width of the diffuser from the hub wall, the shroud wall and both sides. The main conclusions taken from their work are reduction in secondary flows and an increase in compressor performance by reducing diffuser width.

[Ludtke \(1983\)](#) had worked on parallel wall, narrow, constant area tapered and reduced area vaneless diffusers. Their results have shown optimum performance with tapered diffuser. They also concluded that surge of the compressor can be improved without changing diffuser without modifying impeller of the compressor. [Saaresti et al. \(2009\)](#) also performed experiments with reduced diffuser. They concluded that the compressor output is achieved by reduced width in terms of efficiency and pressure increase. [Engeda \(2002\)](#) had carried out experiments with different diffuser widths. His results showed that by increasing the width of the diffuser, there was an acceptable output at lower flow levels. The claims of [Saaresti et al. \(2009\)](#) and [Engeda](#) statements contradicts one another.

Since the effect on the diffuser pressure increase is lower with decreasing or increasing width of the diffuser. Further research is therefore being discussed on rotating diffusers. The walls of the vaneless diffuser are rotated at the same or different impeller speeds. Depending on rotational speed, they are classified into two types. In the case of forced rotation, the diffuser rotates at the same speed as the impeller, which is achieved by the shroud extension or trimming of the blades. The other is free rotation, with diffusers rotating at different speeds than impeller speed known as free rotation.

[Rodgers et al. \(1975\)](#) were the first authors to introduce the rotating vaneless diffuser concept. They performed experiments using mechanical structures between impeller and diffuser to replace the stationary vaneless diffuser by rotating vaneless diffuser. Authors concluded that by rotating diffuser above speed ratio 0.4, frictional losses are minimized and recovery of pressure is good.

[Seralathan et al. \(2016\)](#) had used low speed compressor to numerically test rotating vaneless diffuser. They analysed rotating diffuser for various extensions of the shroud. The authors concluded that the lower percentage of extension has better efficiency and lower pressure rise, and vice versa for higher extension. Authors have therefore analyzed for various shroud extensions and found optimal cases. With different speed ratios, the same authors [Seralathan et al. \(2017\)](#) analyzed free rotating vaneless diffuser. They concluded that their design had demonstrated optimum performance by the speed ratio of 0.75.

[Fradin \(1975\)](#) explored theoretical and experimental advantages of a low-speed centrifugal compressor from a rotating diffuser. They found that performance improved by 2% to 4.5% overall efficiency. [Sapiro \(1983\)](#) worked on the compressor domain of low speed, low pressure ratio, by forming

vaneless diffuser with trimmed impeller blades in specified steps and the method known as extended shrouds. The effect of variation of centrifugal compressor performance with shroud extension is studied as a function of specific speed. The authors concluded that the compressor acceptable efficiency within flow range, minimal impact on pressure rise and almost no effect on the compressor surge flow with extended shrouds.

The forgoing review reveals that very little work has been reported on diffusers with variable width and rotation. All research in this regard to date has been carried out using low speed compressors. In the apparently lone work reported by [Porika et al. \(2019\)](#) on high-speed compressor, it is found that the high-speed compressor with the rotating diffuser having parallel walls are less efficient than the compressor with stationary wall diffuser. Thus, the authors are motivated to expand their work by tapering the diffuser and examining the combined effect of rotation and taper on the performance of high-speed compressor. This is accomplished by

- 1) Modelling a high-speed compressor with a parallel wall diffuser used for this study as a basis case.
- 2) Tapering walls of 1°-6° vaneless diffuser and running simulations by taking into account stationary tapered vaneless diffuser
- 3) Simulations for rotating tapered vaneless diffusers for 1°-6° are carried out further at last.

2. COMPUTATIONAL METHODOLOGY

2.1 Computational Modelling

The geometry details of centrifugal compressor in this study were provided by GTRE (Gas Turbine Research Establishment) as shown in Fig. 1 and Table. 1. The base case for the current simulations is the compressor equipped with the parallel wall diffuser. The tapered wall diffusers can be generated by varying the hub and shroud profile curves using Eqs. (1) and (2). By varying the taper angle (θ) from 1-6 degrees, in the interval of 1° taper six different tapered diffusers are obtained for the present study.

Tapered wall diffuser equations

$$Z_{hub} = Z_{0_hub} + \tan\theta * (r_{2x} - r_2) \quad (1)$$

$$Z_{shroud} = Z_{0_shroud} + \tan\theta * (r_{2x} - r_2) \quad (2)$$

Compressor is composed of the inlet, impeller and diffuser domain. DESIGN MODELER 17.2 is used for the modeling of compressor shown in Fig. 2.

Hub, shroud and profile curves are exported to ANSYS TURBOGRID 17.2 from ANSYS DM 17.2. Topology placement is achieved by using optimized method by ATM. The ATM Topology system is set to Automatic high rounded trailing edge single splitter. Three-dimensional compressor mesh domain with enlarged view is shown in Fig. 3. Global

size factor, overall expansion rate and passage proportional factors are varied until the fine mesh is obtained with no negative elements. The mesh is refined until the number of bad elements is 0%. Shroud tip clearance is given as normal distance. Diffuser diameter ratio is kept constant at 1.75 in all the modified geometries.

Table 1 Geometry details of the compressor

Parameters	Values
The radial width of impeller eye inlet	27.55mm
Impeller inlet radius	18.50mm
Impeller outlet radius	71mm
No. of blades	Main blades – 8
	Splitter blades –8
Shroud tip clearance	0.3mm
Diffuser Outlet radius	125mm
Diffuser Diameter ratio	1.75
Diffuser axial width	5.23mm
Design efficiency	80%

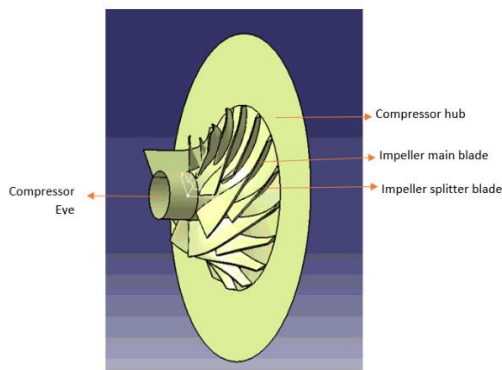


Fig. 2. Schematic centrifugal compressor domain

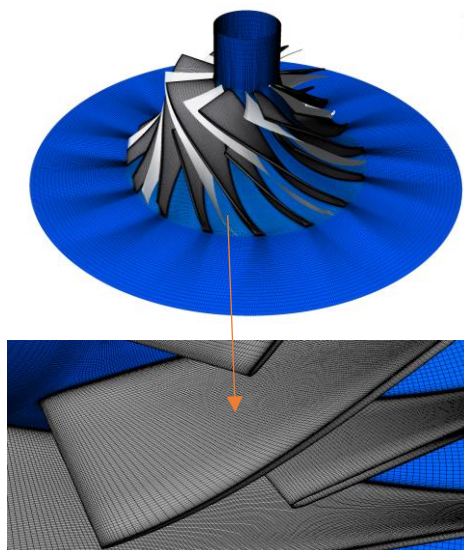


Fig. 3. Compressor Mesh domain with enlarged view of the blades.

2.2 Numerical Solver, Governing Equations and Boundary Conditions

The $k-\omega$ turbulent SST model is used with a high-resolution approach to advection. The same turbulence model was used previously by *Mirzabozorg et al. (2016)*. They achieved optimum results in their work. The time factor is set to one second. Air as ideal gas is used as the fluid medium. Wall condition is imposed for hub, shroud and blade surfaces. The reference pressure is given as zero atmosphere. A frozen rotor interface is used as an interface between the rotor and the stator. The inlet, impeller and diffuser side walls are set to periodic faces, so that simulations can be conducted through a single compressor domain crossing that reduces computational cost and time. Figure 4 indicates the single passage of the compressor domain. Total pressure and total temperature are given as the boundary inlet condition while average static pressure at the choke point and mass flow outlet per component in other working conditions (design to stall) is used as outlet boundary condition.

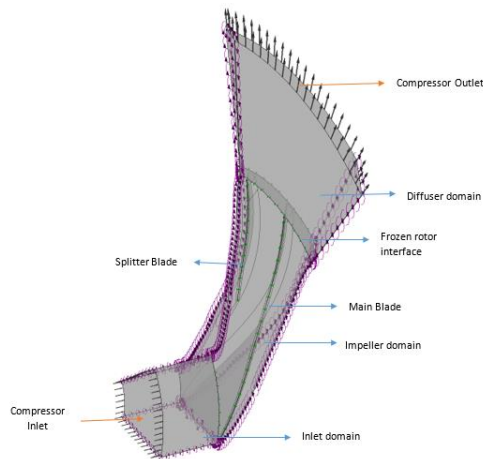


Fig. 4. Single passage of computational domain.

Equations (3) to (7) are the mass, momentum, and energy governing equations are imposed on the compressor ANSYS CFX 17.2 solver. Simulations are assumed to converge when mass, momentum and energy residuals fall below 10^{-5} .

Continuity Equation:

$$\frac{\delta \rho}{\delta t} + \nabla \cdot (\rho, U) = 0 \quad (3)$$

Momentum Equation:

$$\frac{\delta(\rho U)}{\delta t} + \nabla \cdot (\rho U, U) = -\nabla \rho + \nabla \tau + S_M \quad (4)$$

$$\tau = \mu(\nabla U + (\nabla U)^T) - \frac{2}{3} \delta \nabla \cdot U \quad (5)$$

Total Energy Equation:

$$\begin{aligned} \frac{\delta \rho h_{tot}}{\delta t} - \frac{\delta \rho}{\delta t} + \nabla \cdot (\rho U h_{tot}) \\ = \nabla \cdot (\lambda \nabla T) + \nabla \cdot (U \cdot \tau) + U \cdot S_M \\ - S_E \end{aligned} \quad (6)$$

$$h_{tot} = h + \frac{1}{2} U^2 \quad (7)$$

2.3 Numerical Validation

The validation of the numerical solver applied to NASA CC3 compressor with vaned diffuser (Klain, 1997) is shown in Fig. 5. with the experimental results (Lurie et al. 2011). As illustrated in the graph, the agreement between experimental and computational values of total to static pressure ratio is very good. Hence the numerical solver is used for further calculations.

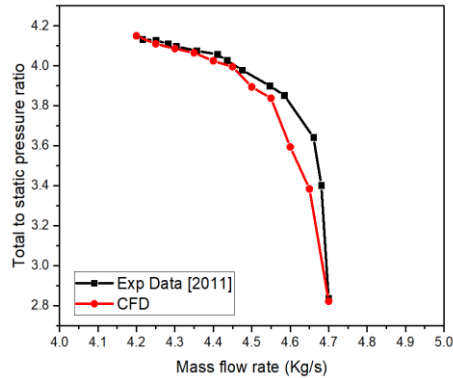
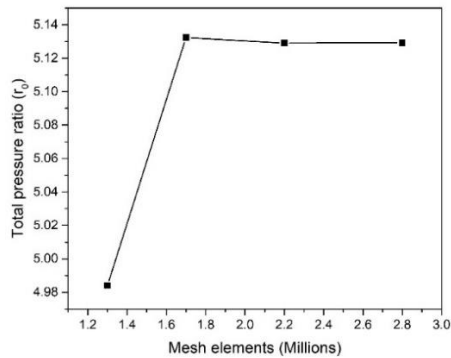


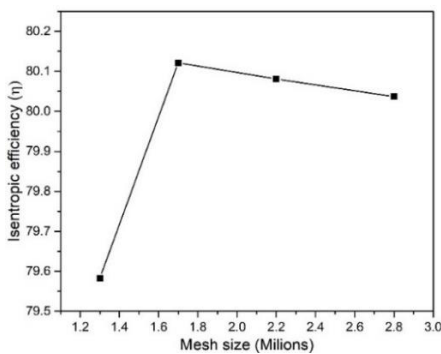
Fig. 5. Numerical Validation of present study.

2.4 Grid Independent Study

Figure 6 shows grid independent study for the geometry currently being considered. The ratio of coarser, medium, and finer mesh elements is kept as 1.3 (Grid convergence index).



a) Total pressure ratio Vs Mass flow rate



b) Isentropic efficiency Vs Mass flow rate

Fig. 6. Grid independent study.

So, a mesh size of 1.7 million elements is considered in the simulations for further study

2.5 Non-Dimensional Performance Characteristics

Following parameters, expressed in Eqs. (8) – (12), taken from previous research (Niveditha et al. 2019) and (Seralathan et al. 2017), are used to compare the performance of various configurations of the compressor with the base model.

Stagnation pressure loss coefficient (C_{P0L}):

$$C_{P0L} = \frac{P_{02} - P_{03}}{0.5 * \rho * U_2^2} \quad (8)$$

Static pressure recovery coefficient (C_P):

$$C_P = \frac{P_3 - P_2}{0.5 * \rho * U_2^2} \quad (9)$$

Coefficient of Torque (C_T):

$$C_T = \frac{T_3 - T_2}{\frac{\pi}{16} \rho U^2 d_o^3} \quad (10)$$

Energy Coefficient (Ψ):

$$\Psi = \frac{C_{U2} * U_2 - C_{U1} * U_1}{0.5 * \rho * U_2^2} \quad (11)$$

Isentropic efficiency:

$$\eta = \frac{\left\{ \left(\frac{P_{03}}{P_{01}} \right)^{\frac{\mu-1}{\mu}} - 1 \right\} * T_{01}}{T_{03} - T_{01}} \quad (12)$$

- P Static pressure
- P_0 Stagnation pressure
- T Torque
- T_0 Total temperature
- U Peripheral velocity
- μ Dynamic viscosity
- 1 Compressor inlet
- 2 Diffuser inlet
- 3 Diffuser outlet

3. RESULTS AND DISCUSSIONS

Unconventional diffuser designs (with the tapered walls, the rotating walls and the combined taper and rotation) are implemented with the aim to improve compressor efficiency and to reduce energy losses.

The machine with parallel wall diffuser is the conventional design and is considered as the base case. Three dimensional simulations were carried out for both the conventional and modified designs in steady state with an impeller speed of 79,000rpm and pressure ratio of 3.2. The tapered diffuser is rendered

Table 2 Computational matrix of the present study

Type	Parameter	Inlet boundary		Outlet boundary		Taper angle	Speed of diffuser (rpm)	No. of cases
		T ₀ (°C)	P ₀ (bar)	m (kg/s)	P _{avg} (kpa)			
Parallel wall diffuser (base case)	-	25	0.99	0.80, 0.78, 0.75, 0.70, 0.65	120, 150, 200, 250	-	-	9
Tapered wall diffuser	Tapered_SVD	25	0.99	0.80, 0.78, 0.75, 0.70, 0.65	120, 150, 200, 250	1°, 2°, 3°, 4°, 5°, 6°	-	54
	Tapered_RVD	25	0.99	0.80, 0.78, 0.75, 0.70, 0.65	120, 150, 200, 250	1°, 2°, 3°, 4°, 5°, 6°	79,000	54

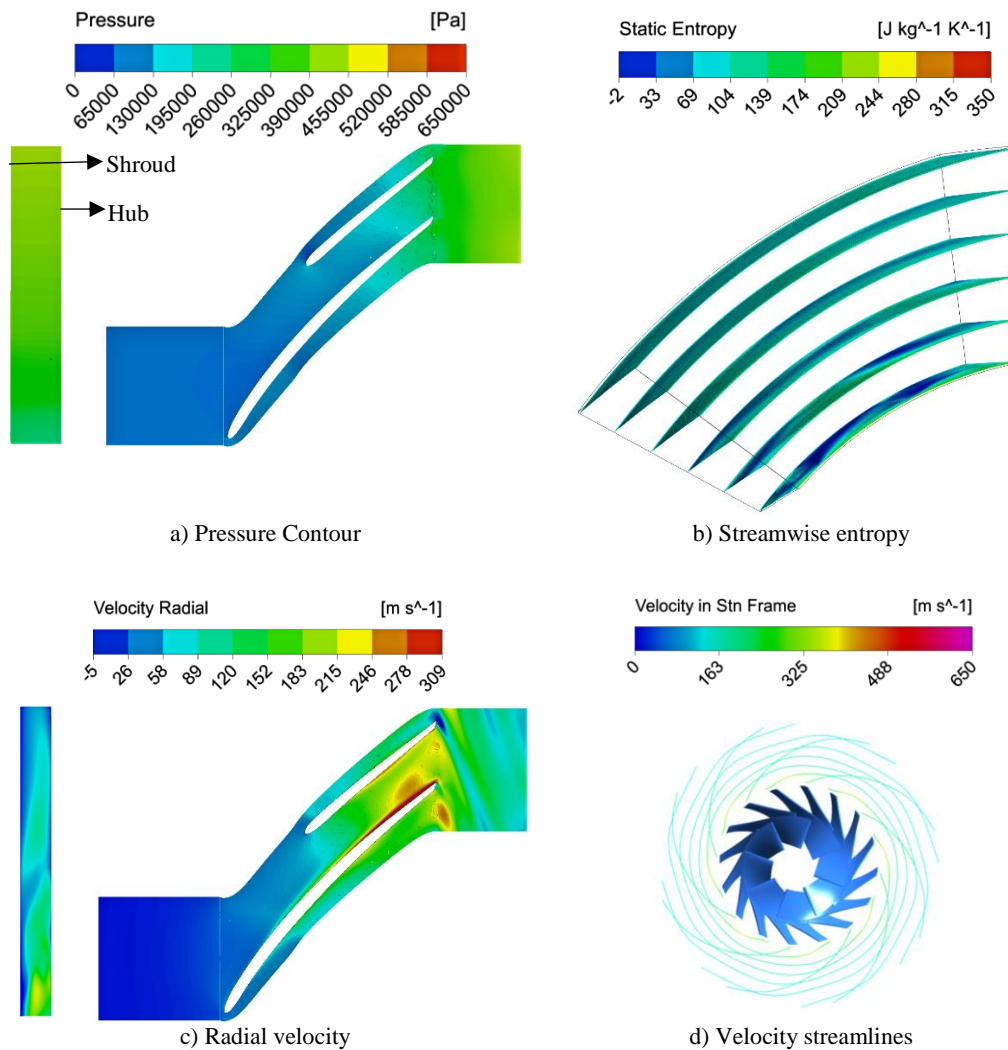


Fig. 7. Contours corresponding to base case (SVD, parallel wall diffuser).

by using Eqs. (1) and (2) to adjust the diffuser hub and shroud curves.

The contours corresponding to base model are shown in Fig. 7 which are used for the comparison with the results of modified geometries. For other simulations, the parallel wall diffuser is replaced by a tapered wall diffuser. First step, the tapered

stationary wall diffuser should be simulated. As the pressure rise in the tapered diffuser is lower than the base case, Additional simulations are given with rotating tapered walls. The computational matrix for the present analysis is shown in Table 2.

Non-dimensional performance characteristics are plotted to quantify the improvement with modified

geometry as compared to the base model. Performance characteristics such as static pressure recovery coefficient (C_p), Stagnation pressure loss coefficient (C_{POL}), Energy coefficient (ψ), Coefficient of torque (C_T) and isentropic efficiency (η) are plotted using Eq. (8) to Eq. (12) in each case. The plotted graphs are validated using static pressure contours, radial velocity contours, streamwise entropy contours and velocity streamlines are plotted at the design point in each case discussed in the following section.

3.1 Static Pressure Recovery Coefficient (C_p)

The coefficient of static pressure recovery gives the pressure recovery in the diffuser. Comparative curves between the tapered and parallel wall diffusers (SVD) of static pressure recovery coefficients are shown in Fig. 8. The pressure recovery for the entire flow range of taperedSVD1 and taperedSVD2 has not improved compared with the base model. In taperedSVD1 and taperedSVD2, pressure recovery in choke mass flow is less than the base case. With taperedSVD3, taperedSVD4, taperedSVD5 and taperedSVD6 static pressure recovery coefficient (C_p) increases for the entire flow range. Static pressure recovery coefficient (C_p) follows a thumb rule: static pressure recovery coefficient (C_p) increases by increasing the taper angle of the diffuser, because of the increase in the diffusion field.

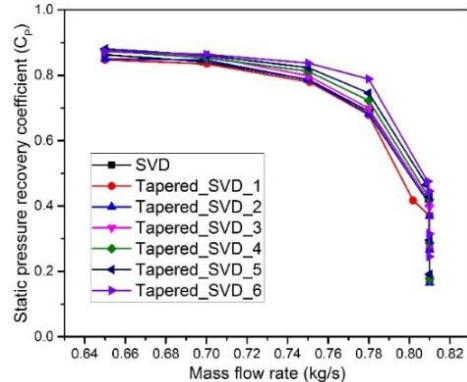


Fig. 8. Static pressure recovery coefficient Vs mass flow rate for Tapered SVD

Increasing static pressure recovery coefficient of taperedSVD3, taperedSVD4, taperedSVD5 and taperedSVD6 by 2.8% – 9.02%, 8.41% – 11.0%, 4.66% – 7.86% and 6.34%–37.57% for each of the respective flow ranges. The static pressure is higher in taperedSVD6 and lower in taperedSVD1 for all the operating conditions. Figure 9 displays pressure contours of stationary tapered diffuser (1° - 6°) in blade to blade view compressor domain and meridional view of diffuser.

The same findings can be seen in Fig. 9, as stated in static pressure recovery coefficient (C_p) Fig. 8: Pressure recovery increase with an increase in diffuser taper angle. In taperedSVD6, the pressure increase is higher and in taperedSVD1 lower. The

flow area of the diffuser increases with tapering the diffuser walls, which decreases velocity and increases diffuser pressure. Which is seen from the meridional view compared to the base model of the diffuser.

Figure 10 shows the coefficient of static pressure recovery of the tapered rotating diffuser comparison with parallel wall diffuser. Curves of static pressure recovery coefficient (C_p) are exactly the other way around for rotating and stationary tapered diffusers. In the case of a rotating tapered diffuser, the higher tapered wall diffuser showed a lower pressure recovery and a higher-pressure recovery is seen in a lower tapered wall diffuser. The rotating walls in the diffuser are adding more energy to the diffuser domain as the diffuser flow passage increases by tapering the additional energy in the diffuser is converted into static pressure recovery. For the cases TaperedRVD1-6, static pressure recovery coefficient increased by 49.75%, 48.45%, 47.32%, 47.12% and 47% respectively at design flow rate of 0.75kg/s.

The Fig. 11 shows the static pressure contours of the meridional diffuser and the compressor blade to blade view corresponding to the rotating diffuser. In case of taperedRVD1 and taperedRVD2, the figure shows clearly that rotating wakes emerge at the diffuser exit. Figure 11 shows secondary flow formation in the rotating tapered diffuser exit because the rotating tapered diffuser has higher pressure recovery as previously stated in Fig. 10 for lower taper angle diffuser. In cases of taperedRVD3, taperedRVD4, taperedRVD5 and taperedRVD6 there is no formation of secondary flows. The wake regions formation in the rotating diffuser reduces isentropic compressor efficiency.

3.2 Energy Coefficient and Coefficient of Torque

Energy coefficient is defined as the relationship between the energy transferred and dynamic head in the compressor. At lower mass flow rates, energy transfer in design to choke flows is less and higher as displayed in Fig. 12. The energy ratio is lower, since the velocity is lower at lower flow rates. Furthermore, as the rate of flow rises is higher, the velocity is higher because of lower pressure, resulting in an increased transfer of energy in the tapered wall diffuser at higher flow rates. taperedSVD1, taperedSVD2, taperedSVD3, taperedSVD4, taperedSVD5 and taperedSVD6 drop and raise energy coefficients by 2.0%-3.32%, 1.26%-24.93%, 0.54%-18.15%, 0.03%-24.93%, 0.76%-15%, and 1.90%-11.58% respectively at lower and higher flow rates.

The contours corresponding to the stationary tapered diffuser cases are shown in Fig. 13. Comparison between Fig. 13 and Fig. 7(b) indicates clearly that in cases of a stationary tapered diffuser the energy generation rates are lower. The entropy generation for taperedSVD1 is lower and in taperedSVD6 the entropy generation is higher compared to the baseline geometry Fig. 7(b).

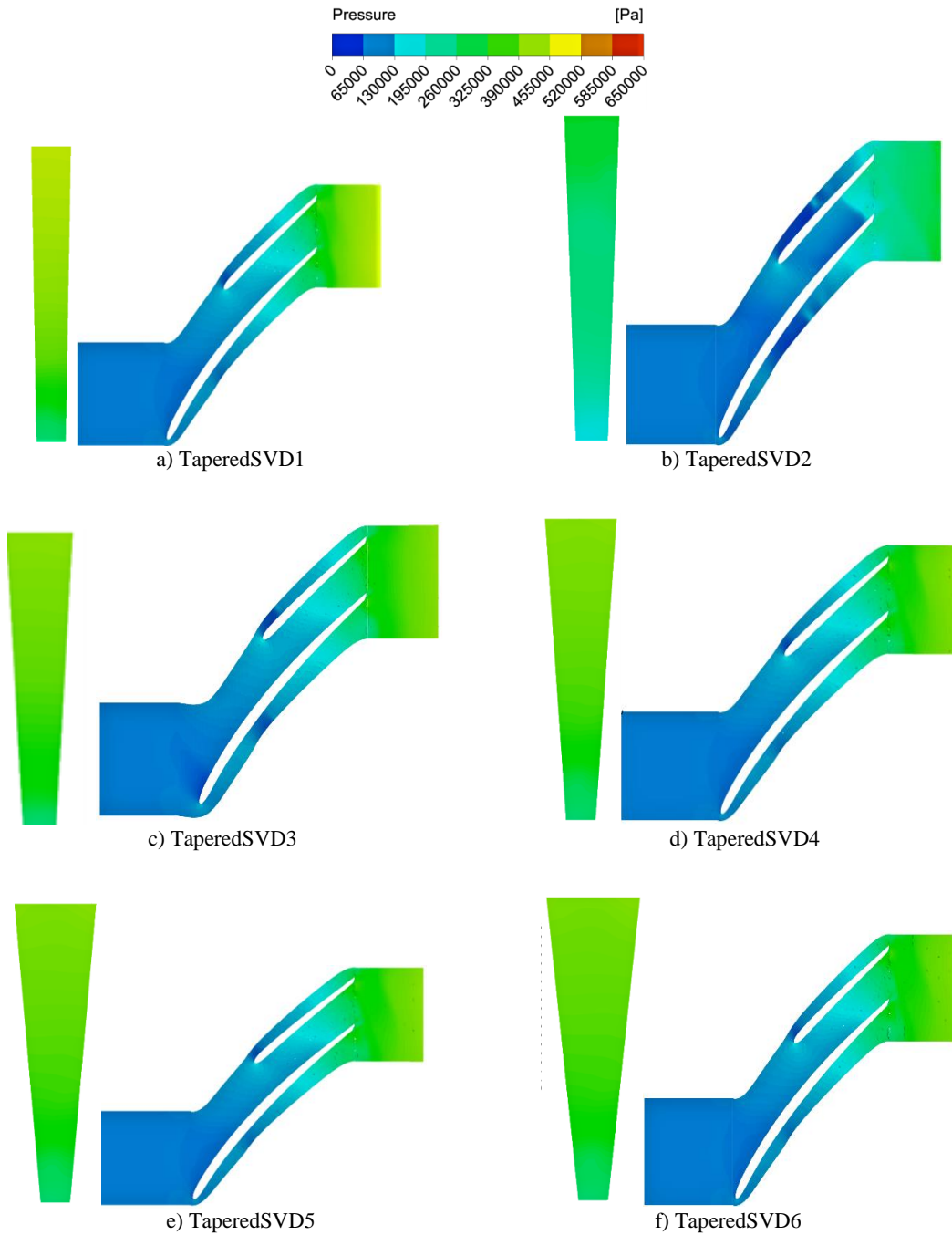


Fig. 9. Pressure Contours corresponding to tapered SVD.

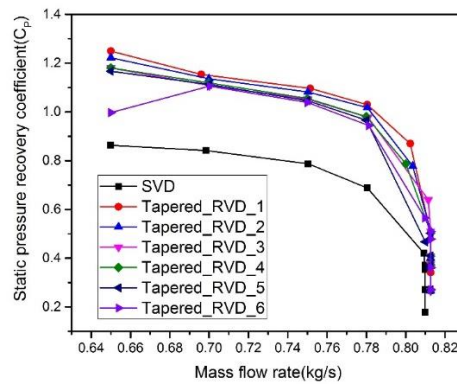


Fig. 10. Static pressure recovery coefficient Vs mass flow rate for tapered RVD.

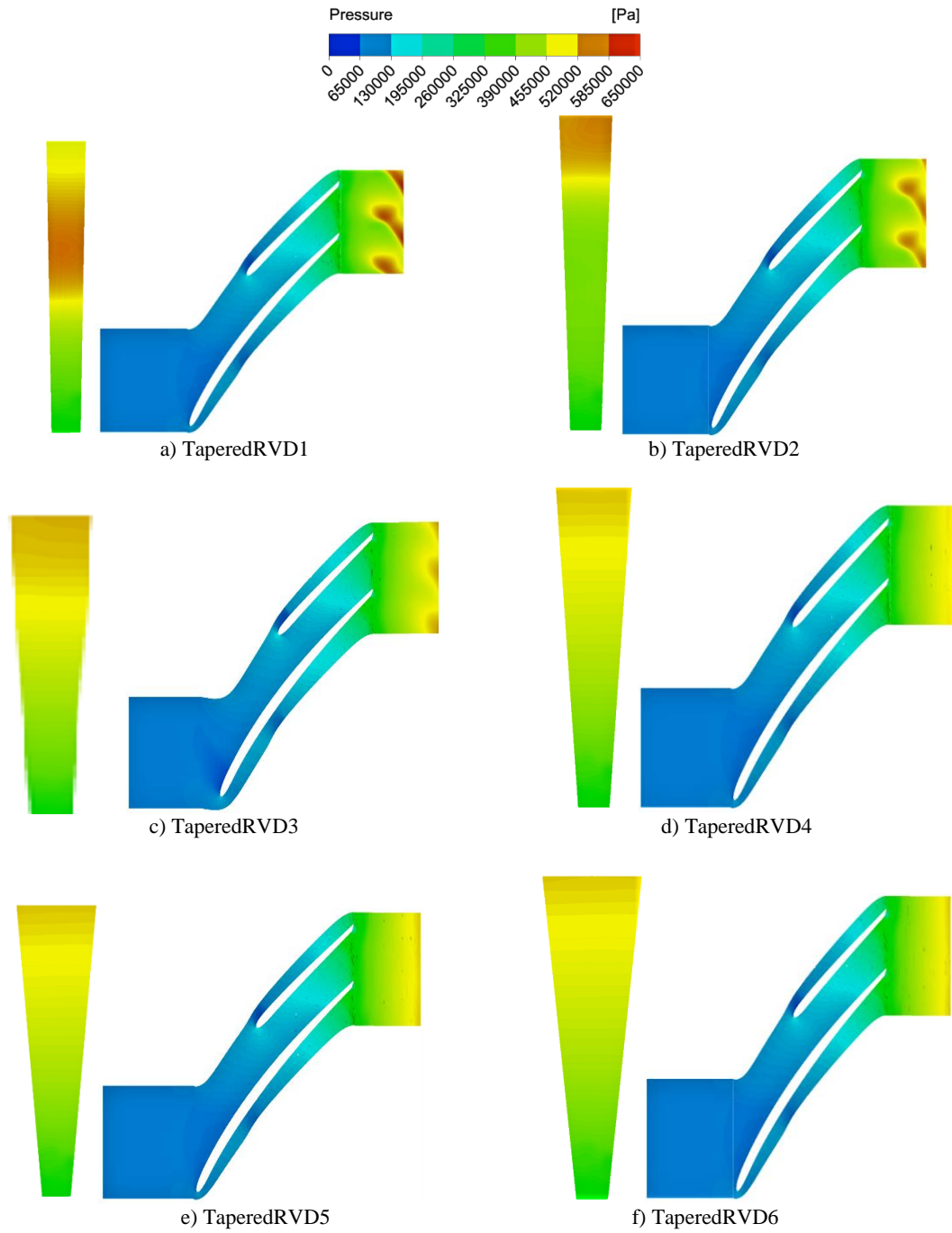


Fig. 11. Pressure contours corresponding to Tapered RVD.

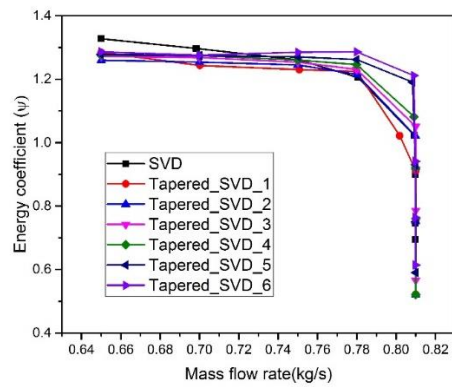


Fig. 12. Energy coefficient Vs mass flow rate.

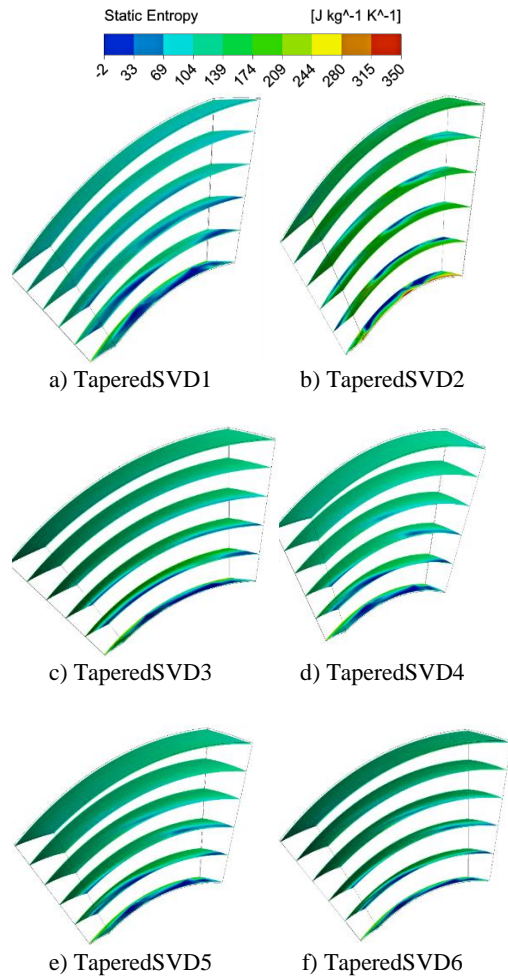


Fig. 13. Streamwise static entropy corresponding to tapered SVD.

Figure 14 shows the coefficient of Torque (C_T) for the rotating tapered diffuser. The torque coefficient is taken into account when energy transformation takes place in the form of rotation for quantitative measurement of the energy transfer rate. Coefficient of Torque (C_T) is lower in cases of taperedRVD1, taperedRVD2, taperedRVD3 and higher in cases of taperedRVD4, taperedRVD5, taperedRVD6 compared to the base model. As described above in static pressure recovery curves (C_p), the pressure recovery is greater in the lower taper angle diffuser than the higher taper angle rotating diffuser. Coefficient of Torque (C_T) decreased by 12.21% - 22.06% and by 8.8% -20.77% respectively in taperedRVD1 and taperedRVD2. Whereas taperedRVD3, taperedRVD4, taperedRVD5 and taperedRVD6 increases in their average flow range by 8.39% - 17.76%, 13.51%-15.06%, 12.06% - 24.15% and 9.06-38.81%, respectively.

The static entropy contours of the rotating tapered diffuser case from 1° to 6° are shown in Fig. 15. TaperedRVD1, taperedRVD2 and taperedRVD3 have a lower entropy generation compared to the generation of baseline entropy. In all instances, the entropy generation of taperedRVD4 is lower. The entropy generation is higher for taperedRVD5 and taperedRVD6. As more energy is applied to the

diffuser walls through rotation, the entropy generation of the rotating tapered diffuser Fig. 15 is larger than the stationary tapered diffuser Fig. 7(b).

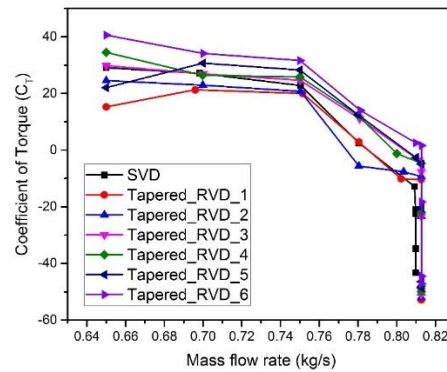


Fig. 14. Coefficient of Torque Vs mass flow rate.

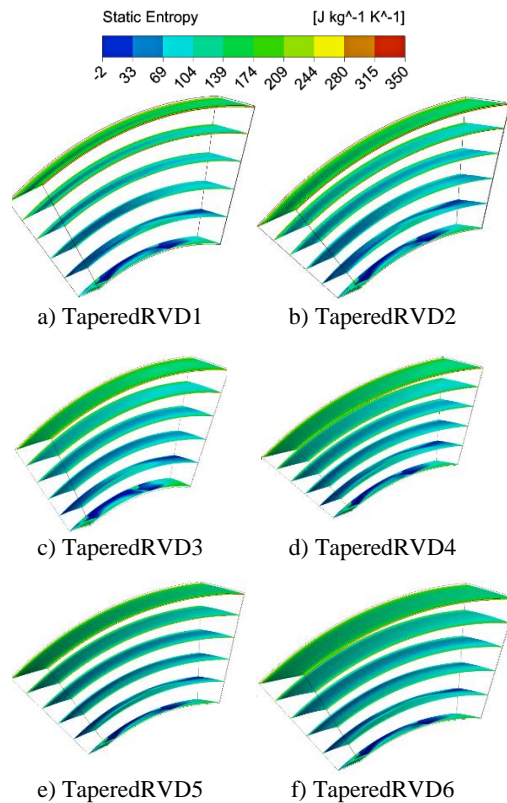


Fig. 15. Streamwise static entropy corresponding to tapered RVD.

3.5 Stagnation Pressure loss coefficient (C_{POL})

The stagnation pressure loss coefficient (C_{POL}) is defined as the ratio of total pressure change through the diffuser to the dynamic head. Figure 16 shows stagnation pressure loss coefficient the curves of corresponding to stationary tapered diffusers. The lowest stagnation pressure loss coefficient was found in taperedSVD3 out of all cases. Stagnation pressure losses decrease with taperedSVD1, taperedSVD2 and taperedSVD3 by 2.93%-4.88%, 2.766-2.69%,

and 4.762%-11.01% respectively for the entire flow range. Whereas in cases of taperedSVD4, taperedSVD5 and taperedSVD6 stagnation pressure loss coefficient increases by 3.24%-4.12%, 6.94%-9.71%, and 10.73%-13.36% respectively over the operating range of the compressor. Stationary tapered diffuser performance curve of stagnation pressure losses shows that even 1° of taper- angle modification in the diffuser has a significant effect on the compressor performance.

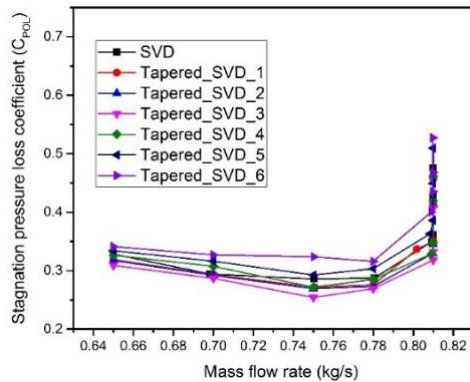


Fig. 16. Stagnation pressure loss coefficient Vs Mass flow rate for Tapered SVD.

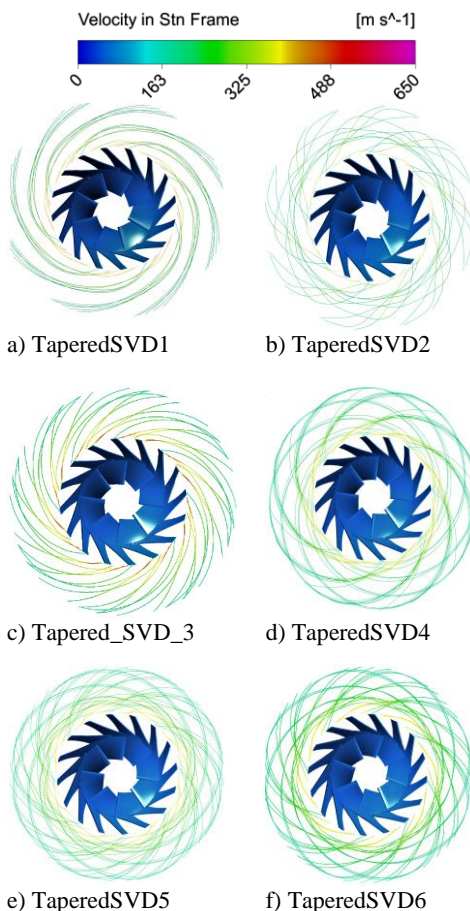


Fig. 17. Velocity Streamlines corresponding to tapered SVD.

Figure 17 displays the velocity streamlines corresponding to the 1°-6° tapering wall diffuser at design flow rates. TaperedSVD3 comprises shorter streamlines, which are consistent and resulting in lower stagnation pressure losses in taperedSVD3. While streamlines of taperedSVD1 and taperedSVD2 are uniform and shorter than that of taperedSVD4, taperedSVD5 and taperedSVD6 but longer than base model streamlines, thus taperedSVD1 and taperedSVD2 has more frictional losses. The Streamlines are longer and non-uniform in the case of taperedSVD4, taperedSVD5 and taperedSVD6 than the base model. As it is well established, shorter and uniform velocity streamlines are preferred over longer and non-uniform streamlines because to overcome frictional losses.

In Fig. 18 comparison of curves with rotating tapered diffuser, stagnation pressure loss coefficient is shown. In taperedRVD1 and taperedRVD2 stagnation pressure losses in comparison with the parallel wall diffuser are higher. As for lower angle tapered diffuser, the static pressure recovery is higher that the secondary flow region is created at the exit of the diffuser. It contributes to increased friction losses in the diffuser domain. Stagnation losses from design to choke are lower for taperedRVD3, although losses from design to surge are higher but lower than the base model. TaperedRVD6 has lower stagnation pressure losses across all rotating tapered diffusers. In taperedRVD1, taperedRVD2 pressure losses increase by 3%-5.5% and 1.48-8.3% respectively, compared to the base model. For taperedRVD3, taperedRVD4, taperedRVD5 and taperedRVD6 stagnation losses decrease by 5% -6.84%, 0.4% -20.75%, 0.95% -9.96% and 1.73% -32.69% respectively compared with the base model.

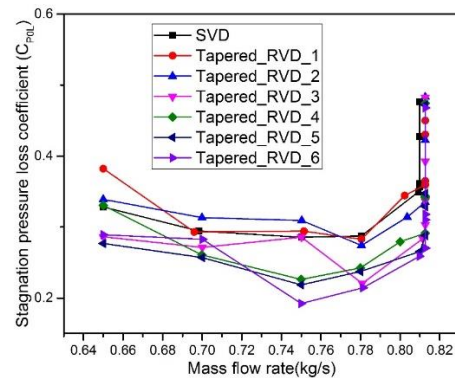


Fig. 18. Stagnation pressure loss coefficient vs mass flow rate for tapered RVD.

The comparison between Fig. 17 and Fig. 19 of standard and rotating tapered diffuser velocity streamlines indicates that velocity streamlines are uniform in contrast to the base model velocity streamlines with a rotating tapered diffuser. The velocity streamlines for taperedRVD1 and taperedRVD2 are longer than the reference geometry. The velocity streamlines are uniform and shorter, as compared with stationary tapered diffuser

cases and baseline geometry, in the case of taperedRVD3, taperedRVD4, taperedRVD5 and taperedRVD6. For all rotating diffuser, the velocity streamlines are identical regardless of the diffuser taper angle since the diffuser shear forces between the walls and the fluid domain are lower by rotating walls, which contributes to lower frictional losses in the rotating diffuser.

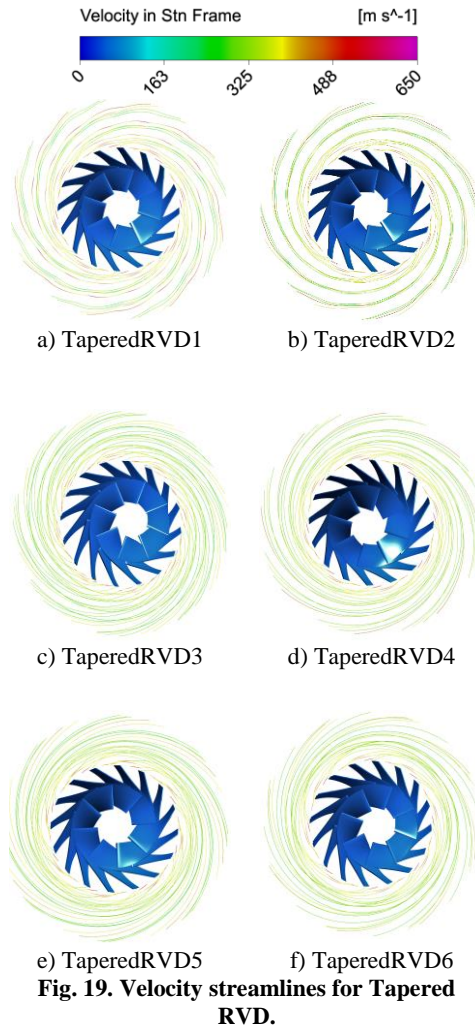


Fig. 19. Velocity streamlines for Tapered RVD.

Figure 20 shows stationary tapered diffuser isentropic efficiency curves. Because Stagnation pressure losses in taperedSVD3 are smaller, the isentropic efficiency of the compressor improved. The Fig. 20 shows that the compressor isentropic efficiency increases in taperedSVD1, taperedSVD2, and taperedSVD3 by 0.69%-1.62%, 0.53%-2.98%—and 0.9%–3.45% respectively over operating range. For the entire flow range of the taperedSVD4 there is no increase or decrease in isentropic efficiency performance. The isentropic efficiency is decreased by 0.98% -2.71% and 0.95% -4.2% in the case of both taperedSVD5 and taperedSVD6, respectively, across the operating range. The higher degree taper angle at choke point demonstrated low performance in comparison with lower degree taper angle diffuser.

The Fig. 21 shows the stationary tapered vaneless diffuser radial velocity contours. Out of all cases, taperedSVD2 has shown higher radial velocity and velocity gradients. The tapering wall of the diffuser does not remove slow-flow regions within the diffuser on the shroud wall caused by the impeller tip clearance. TaperedSVD4, taperedSVD5 and taperedSVD6 are seen with slow flow regions at the diffuser outlet. Better output out of all cases was demonstrated in TaperedSVD1 and TaperedSVD3.

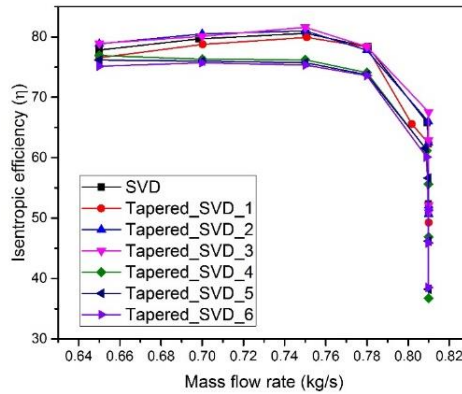


Fig. 20. Isentropic efficiency Vs mass flow rate for Tapered SVD.

Due to the secondary flows in the diffuser which are caused by higher pressure gradients and additional energy transfer, the isentropic efficiency of the compressor is lower in the case of rotating diffuser Niveditha *et al.* (2019). Figure 22 displays isentropic efficiency curves which are comparable to the tapered rotating diffuser. Since the pressure recovery in the lower taper angle is higher and for the higher taper angle the pressure is lower C_p curve RVD Fig. 10, the reverse pattern is observed in the isentropic efficiency of the rotating diffuser as there is no wake area formation with lower pressure recovery. TaperedRVD6 has less efficiency than the base model but greater efficiency than a parallel rotating diffuser. It is therefore possible to conclude that the tapering rotating diffuser walls enhances compressor efficiency. The isentropic efficiency of compressors decreases by 4.8%-14%, 3%-13.03%, 2.65%-12.8%, 3.4%-8.3%, 5.8%-7.4% and 2.9%-7.1% respectively over compressor operating range in cases involving TaperedRVD1, taperedRVD2, taperedRVD3, taperedRVD4, taperedRVD5 and taperedRVD6.

Figure 23 displays the radial velocity contours of the 1°-6° rotating tapered diffuser. The wake region was not shown in the diffuser domain with a higher taper angle diffuser. At the exit of the diffuser domain with lower taper angle diffuser wake regions are formed. Radial velocity in taperedRVD3, taperedRVD4, taperedRVD5 and taperedRVD6 is uniform compared to taperedRVD1 and taperedRVD2 rotating tapered diffusers.

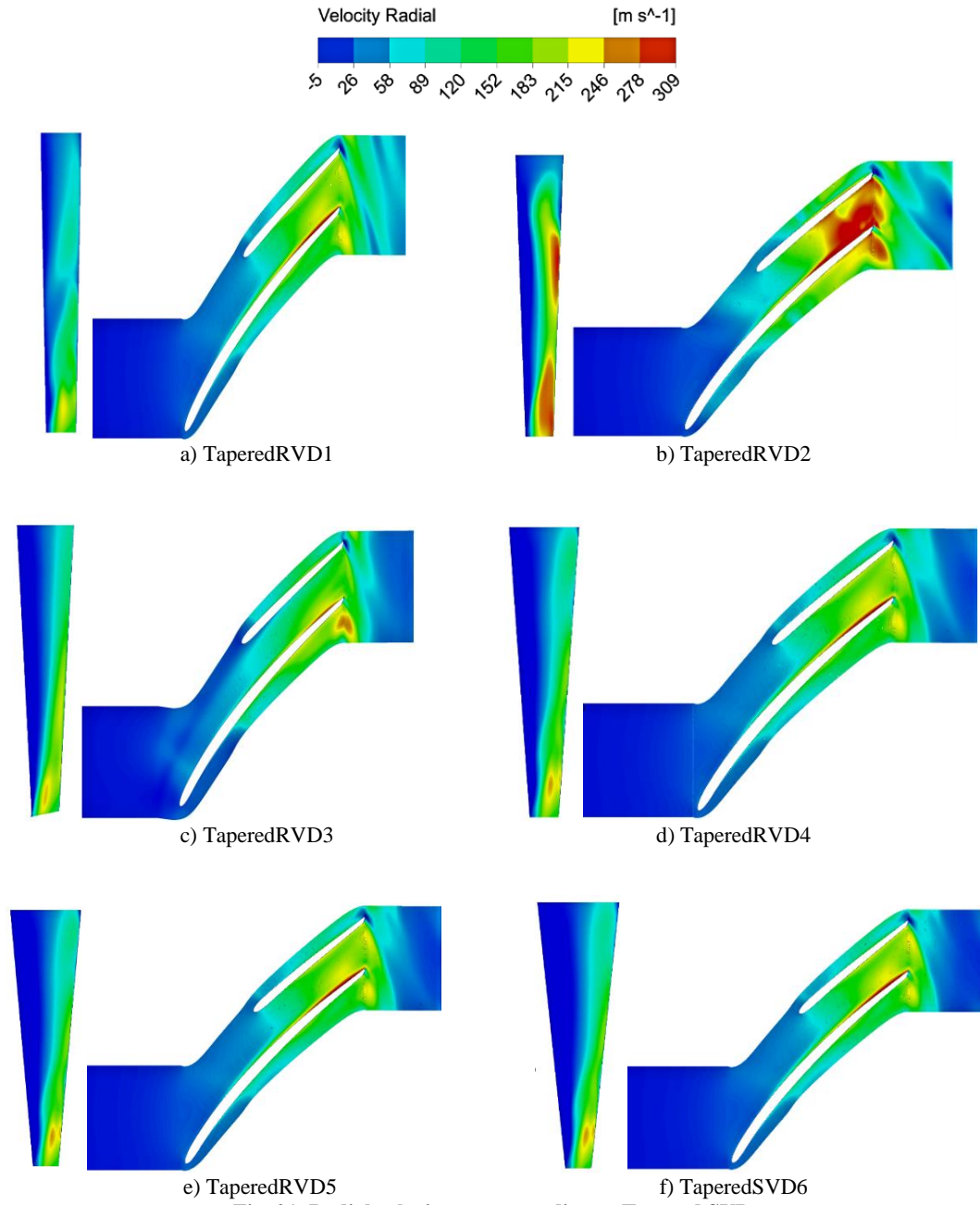


Fig. 21. Radial velocity corresponding to Tapered SVD.

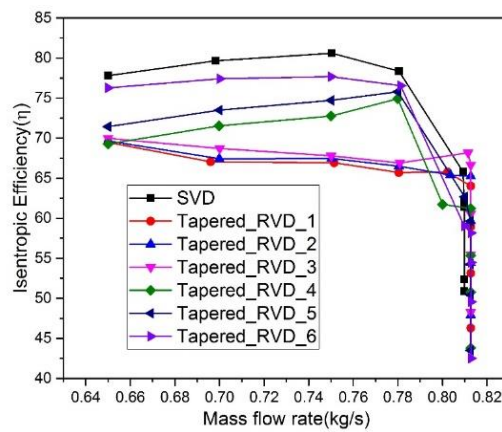


Fig. 22. Isentropic Efficiency Vs Mass flow rate for tapered RVD.

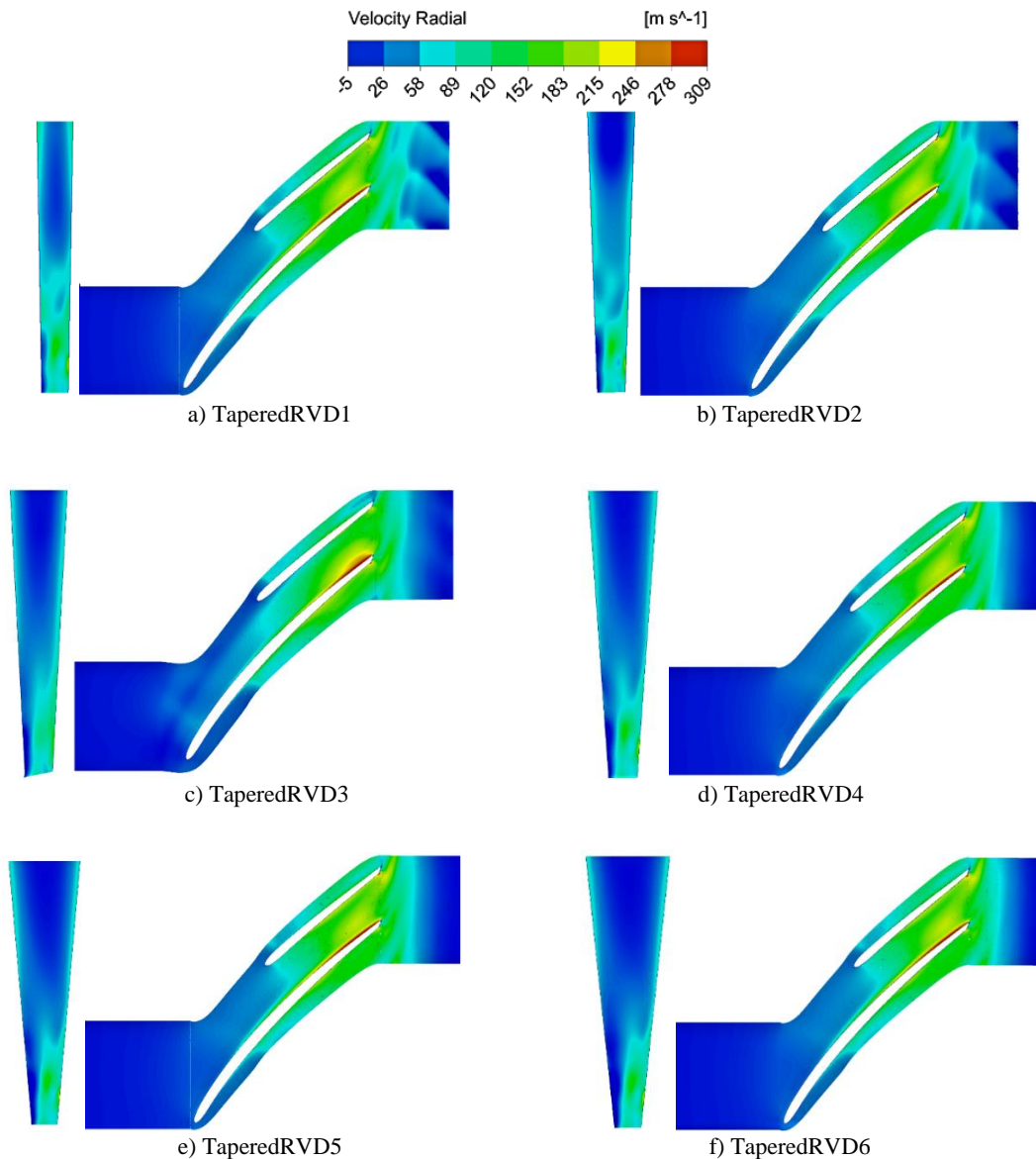


Fig. 23. Radial velocity corresponding to Tapered RVD.

4. CONCLUSIONS

Computational studies on a centrifugal compressor running at 79,000rpm and delivering a pressure ratio of 3.2 are reported. It is shown that the optimum unconventional diffuser designs, with the tapered walls, the rotating walls and with the combined taper and rotation, provided improved performance over the conventional parallel wall diffuser design for the centrifugal compressor. The key findings of the current study are summarized in the following:

1. Static pressure recovery increases by increasing the diffuser taper angle. By rising the taper angle of the diffuser, flow region increases which leads to decrease in flow velocity and increase in static pressure rise.
2. Stationary diffuser with 3° tapered wall had shown an optimum performance by increase in the pressure-ratio and efficiency by 10.7%

and 1.59% respectively.

3. Slow flow region on shroud wall of diffuser caused due to the impeller tip clearance could not be controlled by tapering the diffuser.
4. In the rotating tapered diffuser cases, static pressure recovery is higher compared to the base case of stationary parallel wall diffuser. With the adding of more energy to the diffuser domain, out of all rotating tapered diffuser cases, taperedRVD1 is higher and taperedRVD6 has a lower pressure recovery.
5. The case of taperedRVD6 has shown very little formation of secondary flows inside the diffuser domain. Further the stagnation pressure losses are lower by 32% compared to base case because of uniformity in streamlines. Thus, the performance of rotating tapered wall diffuser is far superior to the rotating parallel wall diffuser.

ACKNOWLEDGEMENT

The authors would like to acknowledge financial support from the project funded by Gas Turbine Research Establishment (GTRE), Defense Research and Development Organization (DRDO), Ministry of Defense, Govt. of India under project COPT (MEE1718384DRDOBVSS). Mr. Shanker Kumar (Scientist F) and Mr. Kishore Kumar (Scientist E) are also acknowledged for providing some insightful comments on this work.

REFERENCES

- Agha Seyed Mirzabozorg, M., M. Bazazzadeh and M. Hamzade (2016). Numerical Study on the Effect of Single Shallow Circumferential Groove Casing Treatment on the Flow Field and the Stability of a Transonic Compressor. *Journal of Applied Fluid Mechanics* 10(1), 257-265.
- Barbaryan, T., S. Hoseinzadeh and P. S. Heyns (2019). Developing a low-fluid pressure safety valve design through a numerical analysis approach, *International Journal of Numerical Methods for Heat & Fluid Flow* 30(3), 1427-1440.
- Chenxing, H., C. Yang, X. Shi, R. Zou, L. Liu and H. Chen (2020). Investigation of rotating stall in radial vaneless diffusers with asymmetric inflow. *Aerospace Science and Technology* 96, 105546.
- Dean, R. C. and Y. Senoo (1960). Rotating wakes in vaneless diffusers. *Journal of Basic Engineering*, 563-570.
- Engeda, A. (2002). The influence of a diffuser width on the unsteady performance of a centrifugal compressor stage. *Proc. of ASME FEDSM.02*, Montreal, Quebec, Canada, FEDSM2002-31250.
- Ferrara, G., L. Ferrari and L. Baldassarre (2004). Rotating Stall in Centrifugal Compressor Vaneless Diffuser: Experimental Analysis of Geometrical Parameters Influence on Phenomenon Evolution. *International Journal of Rotating Machinery* 10(6), 433-442.
- Fradin, C. (1975). The effect of the rotational speed of a vaneless diffuser on the performance of a centrifugal compressor. *European space agency*, Paris, Report no: ESA-TT-202 ONERA-NT-218.
- Hoseinzadeh, S. and P. Stephan Heyns (2020a). Thermo-structural fatigue and lifetime analysis of a heat exchanger as a feedwater heater in power plant. *Engineering Failure Analysis* 113, 104548.
- Hoseinzadeh, S., P. S. Heyns and H. Kariman (2019b). Numerical investigation of heat transfer of laminar and turbulent pulsating Al₂O₃/water nanofluid flow. *International Journal of Numerical Methods for Heat & Fluid Flow* 30 (3), 1149-1166.
- Jaatinen, A., T. Grönman, T. T. Saaresti and P. Røyttä (2011). Effect of vaneless diffuser width on the overall performance of a centrifugal compressor. *Proc. Institution of Mech. Engineering. Part A: Journal of Power and Energy* 225, 665-673.
- Kohzadi, H., A. Shadaram and S. Hoseinzadeh (2018). Improvement of the Centrifugal Pump Performance by Restricting the Cavitation Phenomenon. *Chemical engineering transactions* 71.
- Krain, H. (2005). Review of Centrifugal Compressor's Application and Development. *Journal of Turbomachinery* 127, 24-35.
- Lindner, P. (1983), Aerodynamic Tests on Centrifugal Process Compressors—Influence of Diffuser Diameter Ratio, Axial Stage Pitch, and Impeller Cutback. *Journal of Engineering for Gas turbines and Power* 105(4), 910-919.
- Ludtke, K. (1983), Aerodynamic tests on centrifugal process compressors—the influence of the vaneless diffuser shape. *Journal of Engineering for Gas turbines and Power* 105, 902-909.
- Lurie, E. A., P. R. V. Slooten, G. Medic, J. M. Mulugeta, B. M. Holley, J. Feng and O. Sharma, (2011). Design of a High Efficiency Compact Centrifugal Compressor for Rotorcraft Applications. *American Helicopter Society 67th Annual Forum*, Virginia Beach, USA.
- Mc Klain, T. F. and G. J. Holbrook (1997). Coordinates for a high performance 4:1 pressure ratio centrifugal compressor. *NASA CR-204134*.
- Niveditha, P. and B. V. S. S. Prasad (2019). Numerical Investigation of vaneless diffuser by pinching and rotation, *Proc. ASME Turbo Expo*, Phoenix, Arizona, USA, GT2019-91353.
- Powers, K. H., C. J. Brace, C. J. Budd, C. D. Copeland and P. A. Milewski (2020). Modeling Axisymmetric Centrifugal Compressor Characteristics From First Principles. *ASME. Journal of Turbomachinery* 142(9), 0910.
- Rodgers, C. and H. Mnew (1975). Experiments with a model free rotating vaneless diffuser. *Journal of Engineering for Gas turbines and Power*, 231-241.
- Saaresti, T. T., A. P. Grönman and A. Jaatinen (2009). Experimental study of pinch in vaneless diffuser of centrifugal compressor. *Proc. ASME Turbo Expo*, Florida, USA, GT2009-60162.
- Sapiro, L. (1983). Effect of impeller-extended shrouds on centrifugal compressor performance as a function of specific speed. *ASME Journal of Engineering for Gas turbines and Power* 105, 457-465.
- Senoo, Y. and Y. Kinoshita (1977). Influence of inlet flow conditions and geometries of centrifugal

- vaneless diffusers on critical flow angle for reverse flow. *Journal of Fluids Engineering* (99)1, 98-102.
- Seralathan, S. and D. G. Roy Chowdhury (2016). Performance Enhancement of a Low-Pressure Ratio Centrifugal Compressor Stage with a Rotating Vaneless Diffuser by Impeller Disk Extended Shrouds. *Journal of Applied Fluid Mechanics* 9(6), 2933-2947.
- Seralathan, S. and D. G. Roychowdhury (2017). Numerical Studies on the Effect of Diffuser Rotational Speeds on Low Pressure Ratio Centrifugal Compressor Performance, *Journal of Applied Fluid Mechanics* 10(3), 785-799.
- Sun, Z., X. Zheng and Z. Linghu (2016). Flow Characteristics of a Pipe Diffuser for Centrifugal Compressors. *Journal of Applied Fluid Mechanics* 10(1), 143-155.